metals

MDPI

Article

Improvement in the Hydrogen Storage Properties of MgH_2 by Adding $NaAlH_4$

Young-Jun Kwak [1,2], Myoung-Youp Song [1,2,*] and Ki-Tae Lee [1,2,3]

1 Division of Advanced Materials Engineering, Jeonbuk National University, 567 Baekje-daero, Deokjin-gu, Jeonju 54896, Republic of Korea; twistking18@nate.com (Y.-J.K.); ktlee71@jbnu.ac.kr (K.-T.L.)
2 Hydrogen & Fuel Cell Research Center, Engineering Research Institute, Jeonbuk National University, 567 Baekje-daero, Deokjin-gu, Jeonju 54896, Republic of Korea
3 Department of Energy Storage/Conversion Engineering of Graduate School (BK21 FOUR), Jeonbuk National University, 567 Baekje-daero, Deokjin-gu, Jeonju 54896, Republic of Korea
* Correspondence: songmy@jbnu.ac.kr; Tel.: +82-10-3260-2379

Abstract: Milled MgH_2, MgH_2-10$NaAlH_4$, MgH_2-30$NaAlH_4$, MgH_2-50$NaAlH_4$, and MgH_2-2Ni-10$NaAlH_4$ samples were prepared by milling in a planetary ball mill in hydrogen atmosphere (reactive mechanical milling, RMM). Decomposition temperatures of milled MgH_2, $NaAlH_4$, MgH_2-10$NaAlH_4$, and MgH_2-30$NaAlH_4$ were examined in a Sieverts-type hydrogen absorption and release apparatus, in which the hydrogen pressures were kept nearly constant during hydrogen absorption or release. As the content of $NaAlH_4$ in the sample increased, the temperature at the highest peak in the ratio of increase in released hydrogen quantity to increase in temperature versus temperature curve decreased. Hydriding in 12 bar hydrogen and dehydriding in 1.0 bar hydrogen at 593 K of MgH_2-30$NaAlH_4$ are performed by the reversible reactions $MgH_2 \Leftrightarrow Mg + H_2$ and $17MgH_2 + 12Al \Leftrightarrow Mg_{17}Al_{12} + 17H_2$. MgH_2-30$NaAlH_4$ was the best Mg-based composite among Mg-based alloys in which an oxide, a halide, a fluoride, or a complex hydride was added, with a high hydrogen absorption rate for 2.5 min (2.20 wt% H/min) and a large effective hydrogen storage capacity (7.42 wt% H).

Keywords: hydrogen storage; MgH_2; $NaAlH_4$; decomposition temperature; hydrogen absorption and release rates

check for updates

Citation: Kwak, Y.-J.; Song, M.-Y.; Lee, K.-T. Improvement in the Hydrogen Storage Properties of MgH_2 by Adding $NaAlH_4$. *Metals* **2024**, *14*, 227. https://doi.org/10.3390/met14020227

Academic Editors: Tomasz Czujko, Changlong Tan, Kun Zhang and Yan Feng

Received: 28 December 2023
Revised: 28 January 2024
Accepted: 9 February 2024
Published: 13 February 2024

1. Introduction

Clean alternative energies have drawn interest in preventing air pollution and climate change. One of the clean alternative energies is hydrogen energy, which is the energy produced by the reaction of hydrogen with oxygen, producing water as a by-product. The problems to be solved for applying hydrogen energy to practical use are hydrogen production and storage.

Hydrogen is usually stored in a gaseous state under high pressure and in a cryogenic liquid state. Storing gaseous hydrogen has disadvantages such as safety issues, high cost, and hydrogen embrittlement of storage tank materials. Storage of hydrogen in a cryogenic liquid state has drawbacks such as thermal losses in the case of an open system, safety, and cost of liquefaction.

Another method to store hydrogen is solid-state hydrogen storage using materials such as metal hydrides. Metal hydrides have advantages such as high gravimetric and volumetric storage capacities and safety, as metal hydrides can absorb and release hydrogen at relatively low pressures. Hydrogen is bound by chemical or physical forces in hydrogen storage based on solid-state materials. The technique of storing hydrogen in a solid state has become very attractive and is the subject of studies by many researchers. We are interested in synthesizing metal hydrides based on a metal, magnesium (Mg). Mg-based hydrides have relatively high reaction rates and high hydrogen storage capacities.

Complex hydrides such as $LiBH_4$ and $NaAlH_4$ have been studied by many researchers because they have high theoretical hydrogen storage capacities [1–10]. Many works were performed to improve the hydriding and dehydriding kinetics of Mg [11–16]. Researchers were interested in improving the hydrogen storage properties of MgH_2 by adding $NaAlH_4$ with a high hydrogen storage capacity [17–21]. Ali and Ismail [17] reviewed the hydrogen storage properties of the Mg–Na–Al system. The complex hydride $NaAlH_4$ releases hydrogen via three-step reactions:

$$\text{At } 458 - 503\text{ K}, \quad 3NaAlH_4 \rightarrow Na_3AlH_6 + 2Al + 3H_2 \tag{1}$$

$$\text{At } 533\text{ K}, \quad Na_3AlH_6 \rightarrow 3NaH + Al + (3/2)H_2 \tag{2}$$

$$\text{At } 708\text{ K}, \quad 3NaH \rightarrow 3Na + (3/2)H_2 \tag{3}$$

Ali and Ismail [17] reported that the addition of $NaAlH_4$ could destabilize the MgH_2 effectively and the hydrogen storage properties of $NaAlH_4$ could also be improved by adding MgH_2. The MgH_2-$NaAlH_4$ system exhibited much better dehydriding properties than unary MgH_2 and $NaAlH_4$.

Ismail et al. [20] reported that the following reaction takes place within the temperature range from 443 to 485 K:

$$NaAlH_4 + MgH_2 \rightarrow NaMgH_3 + Al + (3/2)H_2 \tag{4}$$

A mixing decomposition of the reaction of MgH_2 with Al (4) and the decomposition of the excessive MgH_2 (5) occurs reversibly between 553 K and 603 K [20].

$$17MgH_2 + 12Al \Leftrightarrow Mg_{17}Al_{12} + 17H_2 \tag{5}$$

$$MgH_2 \Leftrightarrow Mg + H_2 \tag{6}$$

They also reported that $NaMgH_3$ decomposes between 603 K and 633 K by the following reversible reaction:

$$NaMgH_3 \Leftrightarrow NaH + Mg + H_2 \tag{7}$$

NaH decomposes between 633 K and 648 K by the following reversible reaction [20]:

$$NaH \Leftrightarrow Na + (½)H_2. \tag{8}$$

In the present work, samples with various compositions were prepared and many phenomena were examined such as decomposition temperatures, phase formation, hydrogen absorption and release rates, and hydrogen storage capacity. In addition, the hydrogen storage properties of the prepared samples were compared with those of other Mg-based alloys. In particular, the decomposition temperatures were measured in the Sieverts-type hydrogen absorption and release apparatus, in which the samples were hydrided and dehydrided, by heating the samples at a constant heating rate and simultaneously measuring the released hydrogen quantity. In other researchers' work, the decomposition temperatures were usually measured in thermal analysis instruments such as thermal gravimetric analysis (TGA) and differential scanning calorimetry (DSC). Milled MgH_2, MgH_2-10$NaAlH_4$ (with a composition of 90 wt% MgH_2 + 10 wt% $NaAlH_4$), MgH_2-30$NaAlH_4$ (70 wt% MgH_2 + 30 wt% $NaAlH_4$), MgH_2-50$NaAlH_4$ (50 wt% MgH_2 + 50 wt% $NaAlH_4$), and MgH_2-2Ni-10$NaAlH_4$ (88 wt% MgH_2 + 2 wt% Ni + 10wt% $NaAlH_4$) samples were prepared by milling in a planetary ball mill in hydrogen atmosphere (reactive mechanical milling, RMM). Decomposition temperatures of milled MgH_2, $NaAlH_4$, MgH_2-10$NaAlH_4$, and MgH_2-30$NaAlH_4$ were examined by heating at a rate of 5∼6 K/min in a Sieverts-type hydrogen absorption and release apparatus and phase formation in cycled MgH_2-50$NaAlH_4$ were investigated.

2. Experimental Procedures

As starting materials, we used MgH_2 (magnesium hydride, purity 98%, Alfa Aesar, Ward Hill, MA, USA), $NaAlH_4$ (hydrogen storage grade, Aldrich, St. Louis, MO, USA),

and Ni (average particle size 2.2–3.0 μm, purity 99.9% metal basis, C typically < 0.1%, Alfa Aesar).

Reactive mechanical milling (RMM) was carried out in a planetary ball mill (Planetary Mono Mill; Pulverisette 6, Fritsch). A mixture with the planned composition (total weight = 8 g) was mixed in a stainless steel container (with 105 hardened steel balls, total weight = 360 g) sealed hermetically, the sample-to-ball weight ratio being 1/45. All samples were handled in a glove box in an argon atmosphere. The disc revolution speed was 400 rpm. The mill container (volume of 250 mL) was then filled with high-purity hydrogen gas of about 12 bar. The RMM was performed for 6 h (by repeating milling for 15 min and pausing for 5 min 24 times). Hydrogen was refilled every 2 h (every eight milling times).

The absorbed or released hydrogen quantity was measured as a function of time by a volumetric method, using the Siverts-type hydrogen absorption and release apparatus previously described [16]. The hydrogen pressure in the reactor was kept at 12 bar during hydriding by dosing the quantity of hydrogen absorbed from a reservoir of known volume. The hydrogen pressure in the reactor was kept at 1.0 bar during dehydriding by removing the quantity of hydrogen released from the reactor to a reservoir of known volume. 0.5 g of the samples was used for these measurements. Samples after hydrogen absorption release cycling were characterized by X-ray diffraction (XRD) with Cu Ka radiation, using a Bruker D8 Advance (Karlsruhe, Germany) powder diffractometer.

3. Results

The quantity of released hydrogen, H_r (wt% H), was calculated using the sample weight as a standard.

Figure 1 shows the quantity of released hydrogen (H_r) versus temperature (T) curves and the ratio of increase in H_r to increase in T, dH_r/dT, versus T curves for milled MgH_2, MgH_2-10$NaAlH_4$, MgH_2-30$NaAlH_4$, and $NaAlH_4$ samples. The samples were heated at a heating rate of 5∼6 K/min in 1.0 bar hydrogen. Table 1 presents the temperatures (K) at peaks in the dH_r/dT versus T curves for milled MgH_2, MgH_2-10$NaAlH_4$, MgH_2-30$NaAlH_4$, and $NaAlH_4$ samples. The highest peaks appear at 638, 600, 592, and 455 K, respectively, for milled MgH_2, MgH_2-10$NaAlH_4$, MgH_2-30$NaAlH_4$, and $NaAlH_4$.

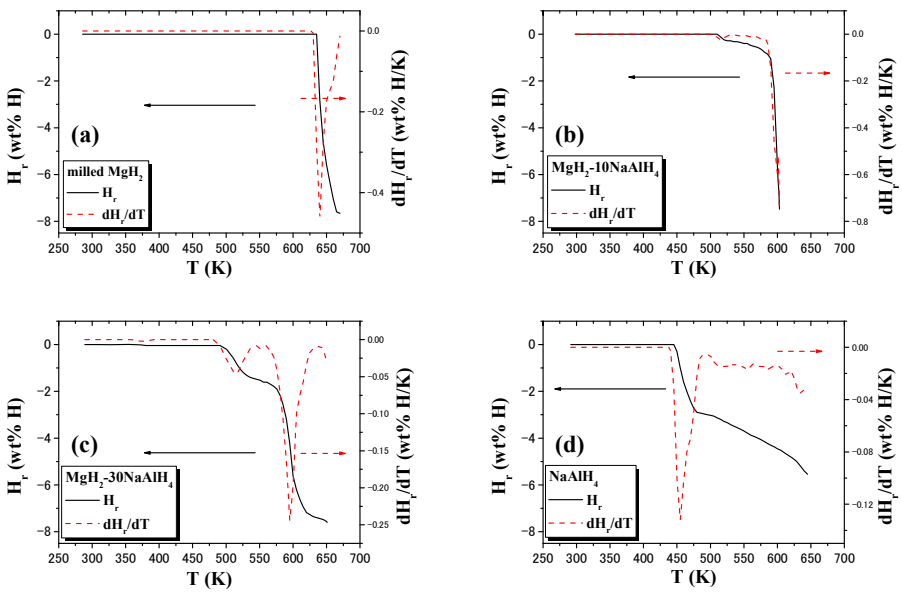

Figure 1. Quantity of released hydrogen (H_r) versus temperature (T) curves and dH_r/dT versus T curves for (**a**) milled MgH_2, (**b**) MgH_2-10$NaAlH_4$, (**c**) MgH_2-30$NaAlH_4$, and (**d**) $NaAlH_4$ samples. The samples were heated at a heating rate of 5∼6 K/min in 1.0 bar hydrogen.

Table 1. Temperatures (K) at peaks in the dH_r/dT versus T curves for milled MgH_2, MgH_2-10$NaAlH_4$, MgH_2-30$NaAlH_4$, and $NaAlH_4$ samples.

	Peak	Highest Peak	Peak	Peak
Milled MgH_2		638		
MgH_2-10$NaAlH_4$	513	600		
MgH_2-30$NaAlH_4$	512	592		
$NaAlH_4$		455	552	631

Figure 2 shows the quantity of released hydrogen (H_r) versus temperature (T) curves for milled MgH_2, MgH_2-10$NaAlH_4$, MgH_2-30$NaAlH_4$, and $NaAlH_4$ samples. The samples were heated at a heating rate of 5∼6 K/min in 1.0 bar hydrogen. The points 1, 2, 3, and 4 were marked so that they correspond to the beginning and ending points of the peaks in Figure 1. Table 2 presents the temperatures (K) at the marked points in the H_r versus T curves for milled MgH_2, MgH_2-10$NaAlH_4$, MgH_2-30$NaAlH_4$, and $NaAlH_4$ samples.

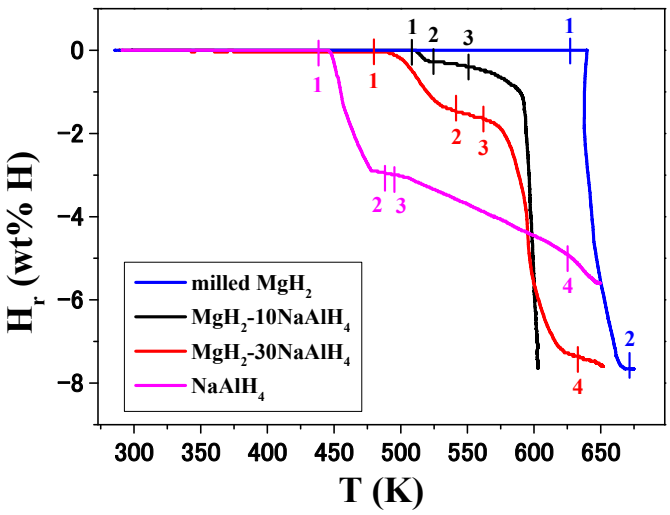

Figure 2. Quantity of released hydrogen (H_r) versus temperature (T) curves for milled MgH_2, MgH_2-10$NaAlH_4$, MgH_2-30$NaAlH_4$, and $NaAlH_4$ samples. The samples were heated at a heating rate of 5∼6 K/min in 1.0 bar hydrogen. The points 1, 2, 3, and 4 were marked so that they correspond to the beginning and ending points of the peaks in Figure 1.

Table 2. Temperatures (K) at the marked points in the H_r versus T curves for milled MgH_2, MgH_2-10$NaAlH_4$, MgH_2-30$NaAlH_4$, and $NaAlH_4$ samples.

Marked Points	1	2	3	4
Milled MgH_2	627	673		
MgH_2-10$NaAlH_4$	508	525	550	
MgH_2-30$NaAlH_4$	480	541	562	633
$NaAlH_4$	438	488	495	625

Hydrogen release begins at 627 K for the as-milled MgH_2. Hydrogen release from the $NaAlH_4$ begins at 438 K and the slope of the H_r versus T curve then changes at 488, 495, and 625 K. MgH_2-10$NaAlH_4$ begins to release hydrogen at 508 K and slopes of the H_r versus T curves change at 525 K and 550 K. MgH_2-30$NaAlH_4$ begins to release hydrogen at 480 K and slopes of the H_r versus T curves change at 541, 562, and 633 K.

As the content of $NaAlH_4$ in the sample increases, the temperature at the highest peak decreases. The higher content of $NaAlH_4$ is believed to strengthen the effects of reactive mechanical grinding, lowering the temperatures for the reaction. The effects of reactive

mechanical milling are thought to be the creation of defects, making clean surfaces and cracks, and decreasing particle sizes.

The XRD pattern of MgH_2-50$NaAlH_4$ dehydrided after the number of cycles, n, of 4 at 593 K is shown in Figure 3. The sample contains Al, MgO, Al_3Mg_2, NaH, and $Mg_{17}Al_{12}$. Al, formed from the reaction (4), is believed to react with Mg (formed by the decomposition of MgH_2) and form Al_3Mg_2 and $Mg_{17}Al_{12}$. The $Mg_{17}Al_{12}$ phase belongs to the body-centered cubic system with a space group of I-43m (No. 217). Samples were easily ignited on exposure to the oxygen in the air to obtain the XRD pattern. This led to the formation of a strong peak of MgO and relatively weak peaks of other phases. The broad peak of MgO shows that the particles of MgO are very fine. The large width of the peaks also suggests that the sample has many defects. In the XRD pattern of pure MgH_2, MgO was not found. However, in the XRD pattern of MgH_2-50$NaAlH_4$ after cycling four times, MgO was observed. It is thought that MgO is formed when the sample is exposed to air to obtain the XRD pattern because the particles of the sample are very fine and the surface of the particles are very clean and reactive.

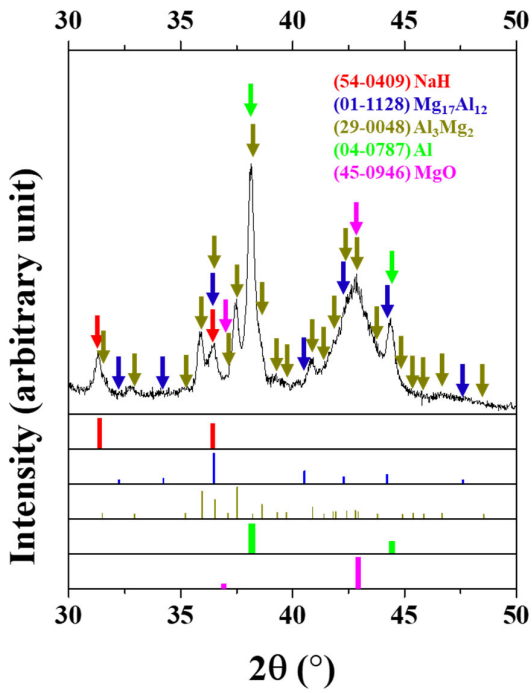

Figure 3. XRD pattern of MgH_2-50$NaAlH_4$ dehydrided after number of cycles, n, of 4 at 593 K. Arrows and bars have the same color as that of a phase.

Liu et al. [22] reported that when the temperature is increased to 633 K, a large amount of hydrogen is released, and two new phases, $Mg_{17}Al_{12}$ and Mg, are formed while the preformed Al and Al_3Mg_2 disappear.

Figure 4 shows the change of H_a versus time t curve at 593 K in 12 bar hydrogen with cycle number, n, for MgH_2-30$NaAlH_4$. The effective hydrogen storage capacity is defined as the quantity of hydrogen absorbed for 60 min (wt% H). As n increases from one to two, the hydrogen absorption rate for 1 min increases. From n = 2 to n = 4, the hydrogen absorption rate for 1 min decreases. In a similar way, the effective hydrogen storage capacity increases as n increases from one to two, and from n = 2 to n = 4, the effective hydrogen storage capacity decreases. The activation is considered to have been completed after n = 2. At n = 2, MgH_2-30$NaAlH_4$ absorbs 4.09 wt% H for 1 min, 7.17 wt% H for 10 min, and 7.42 wt% H for 60 min.

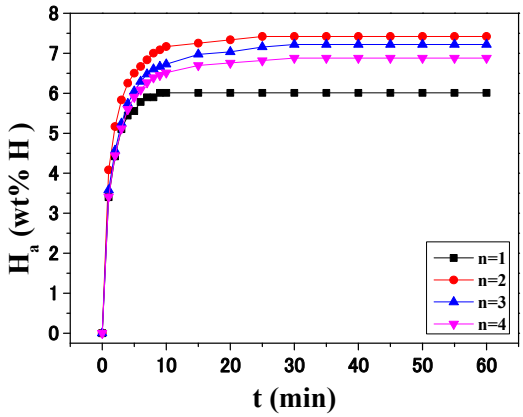

Figure 4. Change in quantity of absorbed hydrogen (H_a) versus time t curve at 593 K in 12 bar hydrogen with cycle number, n, for MgH_2-30$NaAlH_4$.

The change of the H_r versus t curve at 593 K in 1.0 bar hydrogen with n for MgH_2-30$NaAlH_4$ is shown in Figure 5. As the number of cycles (n) increases from one to four, the hydrogen release rate for 1 min decreases. The hydrogen release rate for 1 min at n = 1 and n = 2 are very similar. The quantity of hydrogen released for 60 min increases as n increases from one to two, and from n = 2 to n = 4 the quantity of hydrogen released for 60 min decreases. At n = 2, MgH_2-30$NaAlH_4$ releases 1.31 wt% H for 1 min, 4.95 wt% H for 10 min, and 7.34 wt% H for 60 min.

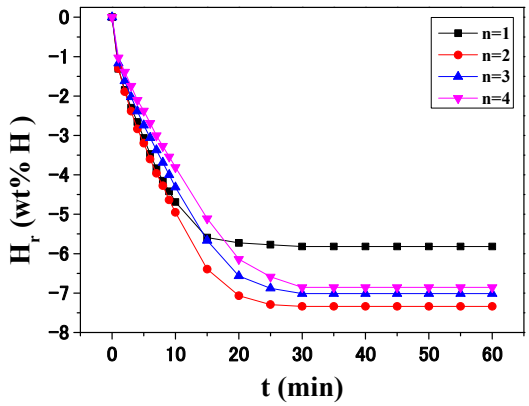

Figure 5. Change in quantity of released hydrogen (H_r) versus t curve at 593 K in 1.0 bar hydrogen with cycle number, n, for MgH_2-30$NaAlH_4$.

Figure 6 shows changes in the H_a versus time t curve at 593 K in 12 bar hydrogen and H_r versus t curve at 593 K in 1.0 bar hydrogen with cycle number, n, for MgH_2-30$NaAlH_4$. The curves show that activation is completed after n = 2, showing the highest hydrogen absorption rate, the highest hydrogen release rate, the largest effective hydrogen storage capacity, and the largest quantity of hydrogen released for 60 min. The curves after completion of activation show that MgH_2-30$NaAlH_4$ has good reversibility and round-trip energy efficiency.

The H_a versus t curves in 12 bar hydrogen at 593 K or 623 K at n = 1 and n = 2 for MgH_2-50$NaAlH_4$ are shown in Figure 7. Because the hydrogen absorption rate was low, experiments were performed several times. Even though the samples were handled in an Ar atmosphere, the samples were ignited partly, leading to low hydrogen absorption rates and low effective hydrogen storage capacities. For n = 1 at 593 K, the MgH_2-50$NaAlH_4$ sample does not absorb hydrogen. For n = 2 at 623 K, the MgH_2-50$NaAlH_4$ sample does not absorb hydrogen either, probably because the difference between the applied hydrogen pressure (12 bar) and the equilibrium plateau pressure at 623 K (6.38 bar [23]) of the Mg-H

system is small. At n = 2, the MgH_2-50$NaAlH_4$ sample absorbs 0.99 wt% H for 1 min, 1.36 wt% H for 10 min, and 3.19 wt% H for 60 min at 593 K.

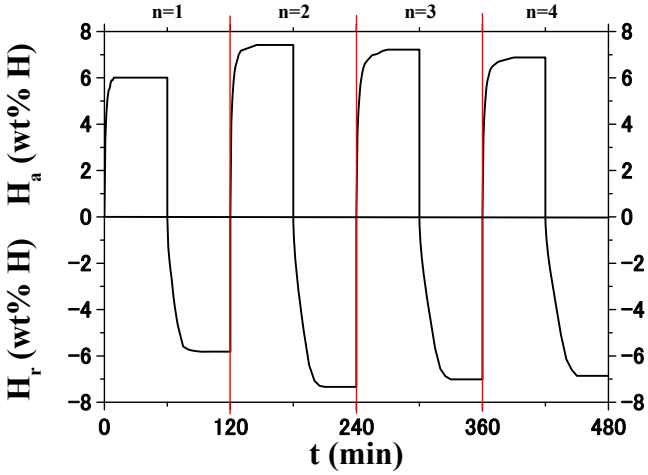

Figure 6. Changes in H_a versus t curve at 593 K in 12 bar hydrogen and H_r versus t curve at 593 K in 1.0 bar hydrogen with cycle number, n, for MgH_2-30$NaAlH_4$.

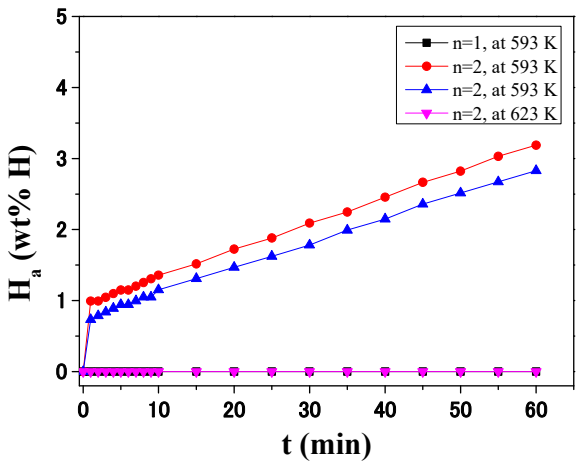

Figure 7. H_a versus t curves in 12 bar hydrogen at 593 K or 623 K at n = 1 and n = 2 for MgH_2-50$NaAlH_4$.

Figure 8 shows the H_r versus t curves in 1.0 bar hydrogen at 593 K or 623 K at n = 1∼4 for MgH_2-50$NaAlH_4$. Hydrogen release rates are low and the quantities of hydrogen released for 60 min are small. As n increases, the initial hydrogen release rate and the quantity of hydrogen released for 60 min increase slightly. At n = 2, the MgH_2-50$NaAlH_4$ sample releases 1.03 wt% H for 5 min and 1.29 wt% H for 60 min at 593 K. When the temperature increases from 593 K to 623 K, the initial hydrogen release rate and the quantity of hydrogen released for 60 min increase slightly. Partial ignition in the samples led to low initial hydrogen release rates and small quantities of hydrogen released for 60 min.

During hydrogen absorption (Figure 3) and release (Figure 4), reactions (5) and (6) are believed to occur.

H_a versus t curves in 12 bar hydrogen at 593 K for activated MgH_2-30$NaAlH_4$, MgH_2-2Ni-10$NaAlH_4$ after RMM, activated Mg-10Fe_2O_3 [24,25], activated Mg-10TaF_5 [26,27], and activated Mg-10VCl_3 [28] are shown in Figure 9. The Mg-10Fe_2O_3 [24,25], Mg-10TaF_5 [26,27], and Mg-10VCl_3 [28] samples were also prepared by RMM under conditions similar to those for preparing MgH_2-30$NaAlH_4$ and MgH_2-2Ni-10$NaAlH_4$. MgH_2-2Ni-10$NaAlH_4$ did not require activation after reactive mechanical milling (RMM). The H_a versus t curve of MgH_2-2Ni-10$NaAlH_4$ after RMM is used for comparison with the H_a versus t curves of other

activated samples. Activated MgH_2-30$NaAlH_4$ has the highest hydrogen absorption rate for 2.5 min, followed in order by MgH_2-2Ni-10$NaAlH_4$ after RMM, activated Mg-10VCl_3, activated Mg-10TaF_5, and activated Mg-10Fe_2O_3. Activated MgH_2-30$NaAlH_4$ has the highest effective hydrogen storage capacity, followed in order by activated Mg-10VCl_3, MgH_2-2Ni-10$NaAlH_4$ after RMM, activated Mg-10Fe_2O_3, and activated Mg-10TaF_5. MgH_2-30$NaAlH_4$ has a much higher hydrogen absorption rate for 2.5 min (2.20 wt% H/min) and a much larger effective hydrogen storage capacity (7.42 wt% H) than the other samples.

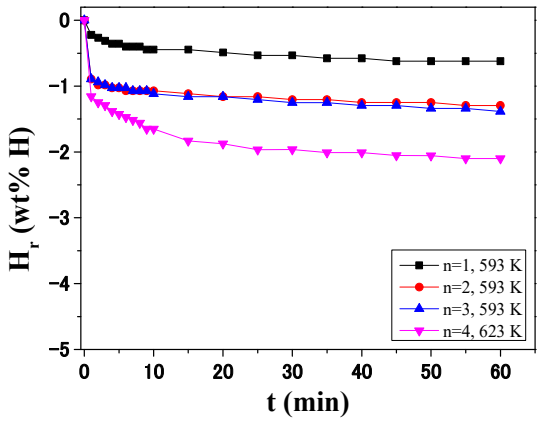

Figure 8. H_r versus t curves in 1.0 bar hydrogen at 593 K or 623 K at n = 1∼4 for MgH_2-50$NaAlH_4$.

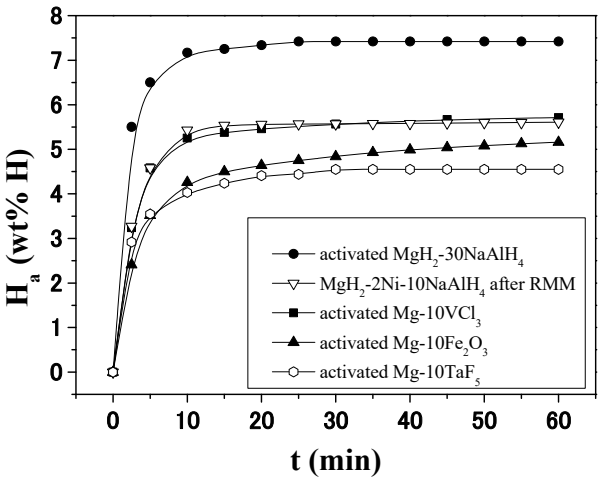

Figure 9. H_a versus t curves in 12 bar hydrogen at 593 K for activated MgH_2-30$NaAlH_4$, MgH_2-2Ni-10$NaAlH_4$ after RMM, activated Mg-10Fe_2O_3, activated Mg-10TaF_5, and activated Mg-10VCl_3.

Figure 10 shows H_r versus t curves in 1.0 bar hydrogen at 593 K for activated MgH_2-30$NaAlH_4$, MgH_2-2Ni-10$NaAlH_4$ after RMM, activated Mg-10Fe_2O_3 [24,25], activated Mg-10TaF_5 [26,27], and activated Mg-10VCl_3 [28]. Activated MgH_2-30$NaAlH_4$ has the highest hydrogen release rate for 2.5 min, followed in order by activated Mg-10VCl_3, activated Mg-10TaF_5, MgH_2-2Ni-10$NaAlH_4$ after RMM, and activated Mg-10Fe_2O_3. Activated MgH_2-30$NaAlH_4$ has the largest quantity of hydrogen released for 60 min, followed in order by activated Mg-10VCl_3, MgH_2-2Ni-10$NaAlH_4$ after RMM, activated Mg-10TaF_5, and activated Mg-10Fe_2O_3, and activated. MgH_2-30$NaAlH_4$ has a much higher hydrogen release rate for 2.5 min (0.86 wt%/min) and a much larger quantity of hydrogen released for 60 min (7.34 wt% H) than the other samples.

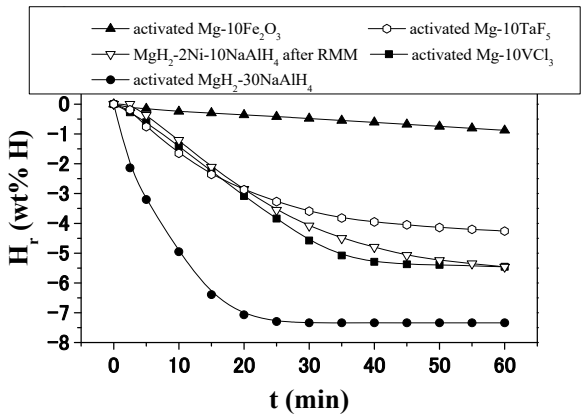

Figure 10. H_r versus t curves in 1.0 bar hydrogen at 593 K for activated MgH_2-30$NaAlH_4$, MgH_2-2Ni-10$NaAlH_4$ after RMM, activated Mg-10Fe_2O_3, activated Mg-10TaF_5, and activated Mg-10VCl_3.

Table 3 shows hydrogen absorption properties in 12 bar hydrogen at 593 K for activated MgH_2-30$NaAlH_4$, MgH_2-2Ni-10$NaAlH_4$ after RMM, activated Mg-10Fe_2O_3 [24], activated Mg-10TaF_5 [26], and activated Mg-10VCl_3 [28]. Numbers in parentheses indicate rankings. H_a (x min) (wt% H) means the quantity of hydrogen absorbed for x min. The initial hydrogen absorption rate is defined as the hydrogen absorption rate during 2.5 min and calculated by dividing H_a (2.5 min) by 2.5 min. Activated MgH_2-30$NaAlH_4$ has the highest initial hydrogen absorption rate, followed in order by MgH_2-2Ni-10$NaAlH_4$ after RMM, activated Mg-10VCl_3, activated Mg-10TaF_5, and activated Mg-10Fe_2O_3. Activated MgH_2-30$NaAlH_4$, MgH_2-2Ni-10$NaAlH_4$ after RMM, and activated Mg-10VCl_3 have relatively large values of H_a (10 min). Activated MgH_2-30$NaAlH_4$ has the highest effective hydrogen storage capacity, followed in order by MgH_2-2Ni-10$NaAlH_4$ after RMM, activated Mg-10VCl_3, activated Mg-10Fe_2O_3, and activated Mg-10TaF_5.

Table 3. Hydrogen absorption properties in 12 bar hydrogen at 593 K for activated MgH_2-30$NaAlH_4$, MgH_2-2Ni-10$NaAlH_4$ after RMM, activated Mg-10Fe_2O_3 (adapted from Ref. [24]), activated Mg-10TaF_5 (adapted from Ref. [26]), and activated Mg-10VCl_3 (adapted from Ref. [28]). Rankings are indicated in parentheses.

Sample	Initial Hydrogen Absorption Rate (wt% H/mn)	H_a (10 min) (wt% H)	Effective Hydrogen Storage Capacity (wt% H)
Activated MgH_2-30$NaAlH_4$	2.20 (1)	7.17 (1)	7.42 (1)
MgH_2-2Ni-10$NaAlH_4$ after RMM	1.31 (2)	5.43 (2)	5.60 (2)
Activated Mg-10Fe_2O_3	0.95 (5)	4.28 (4)	5.16 (4)
Activated Mg-10TaF_5	1.17 (4)	3.82 (5)	4.51 (5)
Activated Mg-10VCl_3	1.26 (3)	5.15 (3)	5.56 (3)

Table 4 shows hydrogen release properties in 1.0 bar hydrogen at 593 K for activated MgH_2-30$NaAlH_4$, MgH_2-2Ni-10$NaAlH_4$ after RMM, activated Mg-10Fe_2O_3 [24], activated Mg-10TaF_5 [26], and activated Mg-10VCl_3 [28]. H_r (x min) (wt% H) means the quantity of hydrogen released for x min. The initial hydrogen release rate is defined as the hydrogen release rate during 2.5 min and calculated by dividing H_r (2.5 min) by 2.5 min. Activated MgH_2-30$NaAlH_4$ has the highest initial hydrogen release rate, followed in order by activated Mg-10VCl_3 and activated Mg-10TaF_5. The initial hydrogen release rates of MgH_2-2Ni-10$NaAlH_4$ after RMM and activated Mg-10Fe_2O_3 are zero. Activated MgH_2-30$NaAlH_4$ has a large value of H_r (10 min). Activated Mg-10TaF_5, activated Mg-10VCl_3, and MgH_2-2Ni-10$NaAlH_4$ after RMM have relatively large values of H_r (10 min). Activated MgH_2-30$NaAlH_4$ has the largest H_r (60 min), followed in order by MgH_2-2Ni-10$NaAlH_4$ after RMM, activated Mg-10VCl_3, activated Mg-10TaF_5, and activated Mg-10Fe_2O_3.

Table 4. Hydrogen release properties in 1.0 bar hydrogen at 593 K for activated MgH_2-30$NaAlH_4$, MgH_2-2Ni-10$NaAlH_4$ after RMM, activated Mg-10Fe_2O_3 (adapted from Ref. [24]), activated Mg-10TaF_5 (adapted from Ref. [26]), and activated Mg-10VCl_3 (adapted from Ref. [28]). Rankings are indicated in parentheses.

Sample	Initial Hydrogen Release Rate (wt% H/mn)	H_r (10 min) (wt% H)	H_r (60 min) (wt% H)
Activated MgH_2-30$NaAlH_4$	0.95 (1)	4.95 (1)	7.34 (1)
MgH_2-2Ni-10$NaAlH_4$ after RMM	0 (4)	1.21 (4)	5.46 (2)
Activated Mg-10Fe_2O_3	0 (4)	0.23 (5)	0.83 (5)
Activated Mg-10TaF_5	0.03 (3)	1.56 (2)	4.01 (4)
Activated Mg-10VCl_3	0.08 (2)	1.32 (3)	5.42 (3)

Table 5 summarizes reversibility, cyclability, round-trip energy efficiency, and general practicability for activated MgH_2-30$NaAlH_4$, MgH_2-2Ni-10$NaAlH_4$ after RMM, activated Mg-10Fe_2O_3, activated Mg-10TaF_5, and activated Mg-10VCl_3. Reversibility (%) is defined as 100 × H_r (60 min)/H_a (60 min) after activation. Cyclability (wt% H/cycle) is defined as the increase in H_a (60 min) per cycle from n =1 to n = 4. Round-trip energy efficiency is defined as H_r (60 min)/H_a (60 min) after activation. General practicability is indicated in ranking by considering all the properties in Tables 3–5. Activated MgH_2-30$NaAlH_4$ has the best reversibility, cyclability, and round-trip energy efficiency, followed in order by MgH_2-2Ni-10$NaAlH_4$ after RMM, activated Mg-10VCl_3, activated Mg-10TaF_5, and activated Mg-10Fe_2O_3. The cyclability of activated MgH_2-30$NaAlH_4$ is positive, showing that H_a (60 min) increases roughly from n = 1 to n = 4.

Table 5. Reversibility, cyclability, round-trip energy efficiency, and general practicability for activated MgH_2-30$NaAlH_4$, MgH_2-2Ni-10$NaAlH_4$ after RMM, activated Mg-10Fe_2O_3, activated Mg-10TaF_5, and activated Mg-10VCl_3. Rankings are indicated in parentheses.

Sample	Reversibility (%)	Cyclability (wt% H/Cycle)	Round-Trip Energy Efficiency	Ranking in General Practicability
Activated MgH_2-30$NaAlH_4$	99 (1)	0.29 (1)	0.99 (1)	1
MgH_2-2Ni-10$NaAlH_4$ after RMM	98 (2)	−0.04 (2)	0.98 (2)	2
Activated Mg-10Fe_2O_3	16 (5)	−0.117 (5)	0.16 (5)	5
Activated Mg-10TaF_5	89 (4)	−0.075 (4)	0.89 (4)	4
Activated Mg-10VCl_3	97 (3)	−0.065 (3)	0.97 (3)	3

Activated MgH_2-30$NaAlH_4$ has the best general practicability, followed in order by MgH_2-2Ni-10$NaAlH_4$ after RMM, activated Mg-10VCl_3, activated Mg-10TaF_5, and activated Mg-10Fe_2O_3. MgH_2-2Ni-10$NaAlH_4$ after RMM has a slightly better general practicability than activated Mg-10VCl_3.

Activated MgH_2-30$NaAlH_4$ has an initial hydrogen absorption rate of 2.20 wt% H/min (vs. 1.26 wt% H/min for activated Mg-10VCl_3), H_a (10 min) of 7.17 wt% H (vs. 5.15 wt% H for activated Mg-10VCl_3), an effective hydrogen storage capacity of 7.42 wt% H (vs. 5.56 wt% H for activated Mg-10VCl_3).

Activated MgH_2-30$NaAlH_4$ has an initial hydrogen release rate of 0.95 wt% H/min (vs. 0.08 wt% H/min for activated Mg-10VCl_3), H_r (10 min) of 4.95 wt% H (vs. 1.32 wt% H for activated Mg-10VCl_3), an H_r (60 min) of 7.34 wt% H (vs. 5.42 wt% H for activated Mg-10VCl_3).

Cyclability in Table 4 is examined only from n = 1 to n = 4. The cyclability of a sample MgH_2-2Ni-10$NaAlH_4$ was examined from n = 1 to n = 30 under 12 bar for hydrogen absorption and 1.0 bar H_2 for hydrogen release at 593 K. MgH_2-2Ni-10$NaAlH_4$ had H_a (60 min) values of 5.62 wt% H at n =1 and 5.36 wt% H at n = 30, showing the good

cyclability of −0.009 wt% H/cycle. The lifetimes of the samples were not investigated. We will examine the lifetimes of the samples in future research.

4. Discussion

From the results of Figure 2, it is believed that for the $NaAlH_4$, reaction (1) (decomposition of $NaAlH_4$) begins to occur at 438 K, and reaction (2) (decomposition of Na_3AlH_6) begins to occur at 495 K. For the MgH_2-10$NaAlH_4$ sample, it is believed that reaction (4) occurs between point 1 (508 K) and point 2 (525 K), reactions (5) and (6) begin to occur after point 3 (550 K), and then reaction (7) and reaction (8) occur consecutively. For the MgH_2-30$NaAlH_4$ sample, it is believed that reaction (4) occurs between point 1 (480 K) and point 2 (541 K), reactions (5) and (6) begin to occur after point 3 (562 K), and then reaction (7) and reaction (8) occur consecutively. The reaction (4) for the MgH_2-30$NaAlH_4$ begins to occur at 28 K lower temperature than that for the MgH_2-10$NaAlH_4$.

Samples were easily ignited on exposure to air, making the obtention of XRD patterns difficult and leading to the formation of a strong peak of MgO and relatively weak peaks of other phases. Liu et al. [22] reported that when the temperature is increased to 633 K, the preformed Al and Al_3Mg_2 disappear. In Figure 3 (the XRD pattern of MgH_2-50$NaAlH_4$ dehydrided after the number of cycles, n, of 4 at 593 K), the Al_3Mg_2 phase is observed. The dehydriding temperature (593 K) lower than that in the work of Liu et al. [22] is believed to have led to this result.

As the content of $NaAlH_4$ in the sample increases, the temperature at the highest peak in the ratio of increase in H_r to increase in T, dH_r/dT, versus T curve decreases. The higher content of $NaAlH_4$ is believed to strengthen the effects of reactive mechanical milling. However, too much content of $NaAlH_4$ (as in MgH_2-50$NaAlH_4$) leads to worse hydrogen storage properties (hydrogen absorption rate, hydrogen release rate, and hydrogen storage capacity).

From the results of this work and the reported study [20], it is believed that hydriding in 12 bar hydrogen and dehydriding in 1.0 bar hydrogen at 593 K of MgH_2-30$NaAlH_4$ are performed by the reversible reactions $MgH_2 \Leftrightarrow Mg + H_2$ and $17MgH_2 + 12Al \Leftrightarrow Mg_{17}Al_{12} + 17H_2$.

In a planetary ball mill, each jar is located on a circular platform (sun wheel). When the sun wheel turns, the jar rotates around its own axis in the opposite direction. The resulting centrifugal and acting acceleration forces lead to strong grinding effects. RMM can break thin surface oxides and expose fresh metallic surfaces, which are reactive. RMM can also introduce defects and cracks. The propagation of cracks, due to additives acting as the center of stress, makes the particles finer. Defects can be used as the sites active for nucleation. The exposed fresh metallic surfaces and created cracks and surfaces have high reactivity. A decrease in particle size reduces the diffusion distance of hydrogen atoms. The added materials and formed phases are believed to strengthen the effects of RMM. The expansion of the lattice due to hydrogen absorption and the contraction of the lattice due to hydrogen release causes effects similar to those of RMM. However, the effects of lattice expansion and contraction will be weaker than those of RMM. The MgH_2-30$NaAlH_4$ sample has a higher hydrogen absorption rate for 2.5 min, a larger effective hydrogen storage capacity, a higher hydrogen release rate for 2.5 min, and a larger quantity of hydrogen released for 60 min than the other samples, showing that the effects of RMM and hydrogen absorption release cycling are stronger in the MgH_2-30$NaAlH_4$ sample, compared with those for the other samples. Reportedly, nucleation can be facilitated by creating active nucleation sites by mechanical treatment and/or alloying with additives [29]; the diffusion distance of hydrogen can also be decreased by the mechanical treatment and/or alloying of Mg with additives, thereby reducing the magnesium particle size [30]. In addition, hydrogen mobility can be improved by additives that create microscopic paths of hydrogen [30]; a rough surface of magnesium particles having many cracks and defects is thus considered more advantageous for hydrogen absorption [31].

In our future work, milled $NaAlH_4$ will be prepared by reactive mechanical milling. The quantity of released hydrogen (H_r) versus temperature T curve and the ratio of increase

in H_r to increase in T, dH_r/dT, versus the T curve for the milled $NaAlH_4$, will be obtained and studied in detail. Behaviors of the milled $NaAlH_4$, which are different from those of $NaAlH_4$, are expected.

As shown in Figures 9 and 10, the additional effects of $NaAlH_4$, oxide, halides, or fluoride on MgH_2 or Mg are different. Which kinds of properties such as physical properties (hardness, toughness, surface area, microstructure, etc.) and chemical properties affect the hydrogen storage properties will be investigated in future work.

5. Conclusions

In the present work, milled MgH_2, MgH_2-10$NaAlH_4$ (with a composition of 90 wt% MgH_2 + 10 wt% $NaAlH_4$), MgH_2-30$NaAlH_4$ (70 wt% MgH_2 + 30 wt% $NaAlH_4$), MgH_2-50$NaAlH_4$ (50 wt% MgH_2 + 50 wt% $NaAlH_4$), and MgH_2-2Ni-10$NaAlH_4$ (88 wt% MgH_2 + 2 wt% Ni + 10wt% $NaAlH_4$) samples were prepared by reactive mechanical milling (RMM). Effects of the $NaAlH_4$ content on the temperatures of intermediate reactions were studied for MgH_2-$NaAlH_4$ composites. Phase formation in the cycled MgH_2-50$NaAlH_4$ was investigated. The hydrogen storage properties of MgH_2-30$NaAlH_4$ were compared with those of Mg-based alloys in which oxide, halides, or fluoride were added. Hydrogen release begins at 627 K for the as-milled MgH_2. MgH_2-30$NaAlH_4$ begins to release hydrogen at 480 K and slopes of the H_r versus T curves change at 541, 562, and 633 K. As the content of $NaAlH_4$ in the sample increased, the temperature at the highest peak in the ratio of increase in H_r to increase in T, dH_r/dT, versus T curve decreased. The higher content of $NaAlH_4$ is believed to have strengthened the effects of reactive mechanical milling. MgH_2-50$NaAlH_4$ dehydrided after four cycles contained Al, MgO, Al_3Mg_2, NaH, and $Mg_{17}Al_{12}$. Hydriding in 12 bar hydrogen and dehydriding in 1.0 bar hydrogen at 593 K of MgH_2-30$NaAlH_4$ are performed by the reversible reactions $MgH_2 \Leftrightarrow Mg + H_2$ and $17MgH_2 + 12Al \Leftrightarrow Mg_{17}Al_{12} + 17H_2$. Activation of MgH_2–30$NaAlH_4$ was completed after two hydrogen absorption release cycles. MgH_2–30$NaAlH_4$ was the best Mg-based composite among Mg-based alloys in which an oxide, a halide, a fluoride, or a complex hydride was added, with a high hydrogen absorption rate for 2.5 min (2.20 wt% H/min) and a large effective hydrogen storage capacity (7.42 wt% H).

Author Contributions: Conceptualization, Y.-J.K., M.-Y.S. and K.-T.L.; methodology, Y.-J.K., M.-Y.S. and K.-T.L.; formal analysis, Y.-J.K., M.-Y.S. and K.-T.L.; investigation, Y.-J.K., M.-Y.S. and K.-T.L.; data curation, Y.-J.K.; writing—original draft preparation, Y.-J.K. and M.-Y.S.; writing—review and editing—Y.-J.K., M.-Y.S. and K.-T.L.; project administration, Y.-J.K. and K.-T.L.; funding acquisition, Y.-J.K. All authors have read and agreed to the published version of the manuscript.

Funding: This work was supported by the National Research Foundation of Korea (NRF) grant funded by the Korean government (MSIT) (No. 2021R1C1C2009103). This work was also supported by Korea Institute of Energy Technology Evaluation and Planning (KETEP) grant funded by the Korean government (MOTIE) (20213030040110).

Data Availability Statement: The original contributions presented in the study are included in the article, further inquiries can be directed to the corresponding author, M.-Y.S.

Conflicts of Interest: The authors declare no conflicts of interest.

References

1. Pratthana, C.; Aguey-Zinsou, K.F. Surfactant Induced Synthesis of $LiAlH_4$ and $NaAlH_4$ Nanoparticles for Hydrogen Storage. *Appl. Sci.* **2022**, *12*, 4742. [CrossRef]
2. Chen, X.; Li, Z.; Zhang, Y.; Liu, D.; Wang, C.; Li, Y.; Si, T.; Zhang, Q. Enhanced Low-Temperature Hydrogen Storage in Nanoporous Ni-Based Alloy Supported $LiBH_4$. *Front. Chem.* **2020**, *8*, 283. [CrossRef] [PubMed]
3. Guo, Y.; Liu, Y.; Feng, L.; An, C.; Wang, Y. High-loading $LiBH_4$ Confined in Structurally Tunable Ni Catalyst-decorated Porous Carbon Scaffold for Fast Hydrogen Desorption. *Chem. Asian J.* **2023**, *18*, 1. [CrossRef]
4. Chen, W.; Sun, Y.; Xu, T.; Ye, J.; Xia, G.; Sun, D.; Yu, X. Reversible Hydrogen Storage Performance of 2$LiBH_4$-MgH_2 Enabled by Dual Metal Borides. *ACS Appl. Energy Mater.* **2022**, *5*, 10501. [CrossRef]
5. Lin, W.; Xiao, X.; Wang, X.; Wong, J.W.; Yao, Z.; Chen, M.; Zheng, J.; Hu, Z.; Chen, L. Extreme high reversible capacity with over 8.0 wt% and excellent hydrogen storage properties of MgH_2 combined with $LiBH_4$ and Li_3AlH_6. *J. Energy Chem.* **2020**, *50*, 296. [CrossRef]

6. Huang, X.; Xiao, X.; He, Y.; Yao, Z.; Ye, X.; Kou, H.; Chen, C.; Huang, T.; Fan, X.; Chen, L. Probing an intermediate state by X-ray absorption near-edge structure in nickel-doped $2LiBH_4$–MgH_2 reactive hydride composite at moderate temperature. *Mater. Today Nano* **2020**, *12*, 100090. [CrossRef]
7. Shen, S.; Liao, W.; Cao, Z.; Liu, J.; Wang, H.; Ouyang, L. Enhanced hydrogen storage properties of MgH_2 with the co-addition of $LiBH_4$ and YNi_5 alloy. *J. Mater. Sci. Technol.* **2024**, *178*, 90. [CrossRef]
8. Shang, Y.; Pistidda, C.; Milanese, C.; Girella, A.; Schökel, A.; Le, T.T.; Hagenah, A.; Metz, O.; Klassen, T.; Dornheim, M. Sustainable $NaAlH_4$ production from recycled automotive Al alloy. *Green Chem.* **2022**, *24*, 4153. [CrossRef]
9. Li, Z.; Yu, J.Z.; Zhang, Y.; Liu, D.M.; Wang, C.Y.; Si, T.Z.; Li, Y.T.; Zhang, Q.A. Coupling of nanoconfinement with metallic catalysis in supported $NaAlH_4$ for low-temperature hydrogen storage. *J. Power Sources* **2021**, *491*, 229611. [CrossRef]
10. Chen, J.; Li, C.; Chen, W.; Zhang, X.; Yu, X.; Xia, G. Tailoring reversible hydrogen storage performance of $NaAlH_4$ through $NiTiO_3$ nanorods. *J. Alloys Compd.* **2024**, *971*, 172689. [CrossRef]
11. Reilly, J.J.; Wiswall, R.H. Reaction of hydrogen with alloys of magnesium and nickel and the formation of Mg_2NiH_4. *Inorg. Chem.* **1968**, *7*, 2254–2256. [CrossRef]
12. Karty, A.; Genossar, J.G.; Rudman, P.S. Hydriding and dehydriding kinetics of Mg in a Mg/Mg_2Cu eutectic alloy: Pressure sweep method. *J. Appl. Phys.* **1979**, *50*, 7200–7209. [CrossRef]
13. Akiba, E.; Nomura, K.; Ono, S.; Suda, S. Kinetics of the reaction between Mg-Ni alloys and H_2. *Int. J. Hydrogen Energy* **1982**, *7*, 787–791. [CrossRef]
14. Bobet, J.-L.; Akiba, E.; Nakamura, Y.; Darriet, B. Study of Mg–M (M = Co, Ni and Fe) mixture elaborated by reactive mechani cal alloying-hydrogen sorption properties. *Int. J. Hydrogen Energy* **2000**, *25*, 987–996. [CrossRef]
15. Huot, J.; Ravnsbæk, D.B.; Zhang, J.; Cuevas, F.; Latroche, M.; Jensen, T.R. Mechanochemical synthesis of hydrogen storage materials. *Prog. Mater. Sci.* **2013**, *58*, 30–75. [CrossRef]
16. Song, M.Y.; Ahn, D.S.; Kwon, I.H.; Ahn, H.J. Development of Hydrogen storage Alloys by Mechanical Alloying Mg with Fe and Co. *Met. Mater. Int.* **1999**, *5*, 485–490. [CrossRef]
17. Ali, N.A.; Ismail, M. Advanced hydrogen storage of the Mg–Na–Al system: A review. *J. Magnes. Alloys* **2021**, *9*, 1111–1122. [CrossRef]
18. Plerdsranoy, P.; Meethom, S.; Utke, R. Dehydrogenation kinetics, reversibility, and reaction mechanisms of reversible hydrogen storage material based on nanoconfined $MgH_2-NaAlH_4$. *J. Phys. Chem. Solids* **2015**, *87*, 16–22. [CrossRef]
19. Rafi-ud-din; Xuanhui, Q.; Ping, L.; Zhang, L.; Ahmad, M.; Iqbal, M.Z.; Rafique, M.Y.; Farooq, M.H. Enhanced hydrogen storage performance for MgH_2–$NaAlH_4$ system—The effects of stoichiometry and Nb_2O_5 nanoparticles on cycling behaviour. *RSC Adv.* **2012**, *2*, 4891–4903. [CrossRef]
20. Ismail, M.; Zhao, Y.; Yu, X.B.; Mao, J.F.; Dou, S.X. The hydrogen storage properties and reaction mechanism of the MgH_2–$NaAlH_4$ composite system. *Int. J. Hydrogen Energy* **2011**, *36*, 9045–9050. [CrossRef]
21. Bendyna, J.K.; Dyjak, S.; Notten, P.H.L. The influence of ball-milling time on the dehydrogenation properties of the $NaAlH_4$–MgH_2 composite. *Int. J. Hydrogen Energy* **2015**, *40*, 4200–4206. [CrossRef]
22. Liu, H.; Wang, X.; Liu, Y.; Dong, Z.; Ge, H.; Li, S.; Yan, M. Hydrogen Desorption Properties of the MgH_2–AlH_3 Composites. *J. Phys. Chem. C* **2014**, *118*, 37–45. [CrossRef]
23. Stampfer, J.F.; Molley, C.E.; Suttle, J.F. The Magnesium-Hydrogen System1-3. *J. Am. Chem. Soc.* **1960**, *82*, 3504–3508. [CrossRef]
24. Song, M.Y.; Kwon, I.H.; Kwon, S.N.; Park, C.G.; Hong, S.-H.; Bae, J.-S.; Mumm, D.R. Hydrogen-storage properties of Mg–oxide alloys prepared by reactive mechanical grinding. *J. Alloys Compd.* **2006**, *415*, 266–270. [CrossRef]
25. Song, M.Y.; Kwon, S.N.; Park, H.R. Pressure-Composition Isotherms and Cycling Properties of Mg-xFe_2O_3-yNi Alloys. *Korean J. Met. Mater.* **2013**, *51*, 455–460. [CrossRef]
26. Kwak, Y.J.; Lee, S.H.; Park, H.R.; Song, M.Y. Review Paper: Hydriding and Dehydriding Reactions of Mg-xTaF_5 (x=0, 5, and 10) Prepared via Reactive Mechanical Grinding. *Korean J. Met. Mater.* **2014**, *52*, 957–962.
27. Kwak, Y.J.; Lee, S.H.; Park, H.R.; Song, M.Y. Hydrogen Storage Characteristics of Mg, Mg-5TaF_5, and Mg-5NbF_5 Prepared via Grinding in a Hydrogen Atmosphere. *J. Nanosci. Nanotechnol.* **2016**, *16*, 10508–10514. [CrossRef]
28. Song, M.Y.; Lee, S.H.; Mumm, D.R. Fe_2O_3, MnO, and VCl_3-added Mg composites by reaction involving grinding processing for hydrogen storage. *J. Ceram. Proc. Res.* **2018**, *19*, 211–217.
29. Hjort, P.; Krozer, A.; Kasemo, B. Hydrogen sorption kinetics in partly oxidized Mg films. *J. Alloys Comp.* **1996**, *237*, 74–80. [CrossRef]
30. Zaluska, A.; Zaluski, L.; Ström-Olsen, J.O. Nanocrystalline magnesium for hydrogen storage. *J. Alloys Comp.* **1999**, *288*, 217–225. [CrossRef]
31. Vigeholm, B.; Kjoller, J.; Larsen, B.; Pedersen, A.S. Formation and decomposition of magnesium hydride. *J. Less-Common Met.* **1983**, *89*, 135–144. [CrossRef]